Powder Technology 256 (2014) 545–552

Contents lists available at ScienceDirect

Powder Technology

journal homepage: www.elsevier.com/locate/powtec

Electrochemical properties of mechanically alloyed Ni-doped FeS_2 cathode materials for lithium-ion batteries

Xiaojing Liu [a], Hye-seong Kim [a], Ji-hyun Hong [a], Zhezhu Xu [b], Hong Xiao [c], In-shup Ahn [a,*], Ki-won Kim [a]

[a] School of Materials Science and Engineering, Gyeongsang National University, 900 Gajwa-dong, Jinju, Gyeongnam 660-701, Republic of Korea
[b] School of Mechanical and Aerospace Engineering, Gyeongsang National University, 900 Gajwa-dong, Jinju, Gyeongnam 660-701, Republic of Korea
[c] School of Power and Energy, Northwestern Polytechnical University Xian, Shaanxi 710-072, China

ARTICLE INFO

Article history:
Received 8 October 2013
Received in revised form 20 November 2013
Accepted 6 January 2014
Available online 13 January 2014

Keywords:
Mechanical alloying (MA)
Nickel-doped iron disulfides
Lithium-ion batteries
Electrochemical properties

ABSTRACT

In this study, fine cathode materials $Fe_{0.8}Ni_{0.2}S_2$ and $Fe_{0.9}Ni_{0.1}S_2$, with mean particle sizes of 3.39 μm and 2.79 μm, respectively, can be prepared simply through mechanical alloying (MA). The contents of nickel show a significant effect on the electrochemical behavior of the composites, as shown the charge/discharge capacity of 320/285 mAh/g is maintained for over 20 cycles for the Li/$Fe_{0.8}Ni_{0.2}S_2$ cell, higher than that for the Li/$Fe_{0.9}Ni_{0.1}S_2$ with 284/233 mAh/g when tested ranging from 0.8 to 2.4 V at 0.1 C. In addition, the electronic conductivity seemed also enhanced with high nickel doping content, leading to the improvement of the cycling stability of the FeS_2 based electrodes.

1. Introduction

Recently, with the increasing popularity of portable electronic products such as cellular phones, laptops, and camcorders and the pressing need for high specific energy storage in aviation, aerospace, electric vehicles and other high-tech fields, lithium-ion batteries, as one source of high specific energy, are becoming the focus of research. However, their development and application have been greatly limited in some areas due to the shortcomings of practical commercial cathode materials ($LiCoO_2$, $LiMn_2O_4$, $LiNiO_2$, etc.), such as poor cobalt resources, bad electrochemical performance at high temperatures, and difficulties in the manufacturing process [1]. Therefore, research and development of new battery systems, especially new cathode materials, are becoming particularly important.

Among the various candidates for cathode materials, metal sulfides, such as TiS_2 [2], CuS [3], Ni_3S_2 [4] and especially FeS_2 [5], have been hailed as the most promising materials during the early stages of the development of secondary batteries, since they are cheap, nontoxic, available in abundance at low cost, and more importantly, can provide high energy density when coupled with lithium [6]. Of course, in addition to the cathode, there are several other factors that can also affect the electrochemical properties of Li-ion cells, such as the size, surface area and surface chemistry of the electrical conductor, the binding properties, flatness, porosity and structural stability of the cathode. However, in terms of the degree of influence on the overall performance of the cells, the mean particle size, size distribution, and structural stability of the cathode material and also the test conditions during the charge/discharge process seem particularly important. Therefore, preparation of the material has become the core of the whole experiment.

Although extensive chemical methods, such as spray pyrolysis synthesis and hydrothermal/solvothermal synthesis, have been used to prepare suitable particles of iron disulfide, by controlling not only the particle morphology and size distribution, but also the crystal structures, the whole electrochemical properties of Li/FeS_2 cells do not appear to be greatly enhanced. In terms of the previous reports, the reasons are diverse and dissimilar, but using cathode material with poor structural stability is the most serious weakness for Li/FeS_2 cells [7]. Therefore, research into new synthesis methods that can improve the structural stability is becoming crucially important.

In this study, we will prepare fine compounds of Ni-doped iron disulfides using a new, simple, effective and convenient process, mechanical alloying (MA), which has not received much attention in the field of lithium-ion batteries (until Disma's early study on raising the electroactivity of lithium through a milling process [8]), yet can provide a way for direct solid-state synthesis and help improve the purity of the resultant substances. Here, in view of the high energy milling machine, the element nickel is expected to replace some atoms or insert some spaces in the lattice, to improve the structural stability of the synthesized materials, therefore enhancing the charge/discharge capacity and cycle life property of the Li/Ni-doped FeS_2 cells.

* Corresponding author. Tel.: +82 55 772 1662; fax: +82 55 772 1745.
E-mail address: ais@gnu.ac.kr (I. Ahn).

http://dx.doi.org/10.1016/j.powtec.2014.01.012
0032-5910/

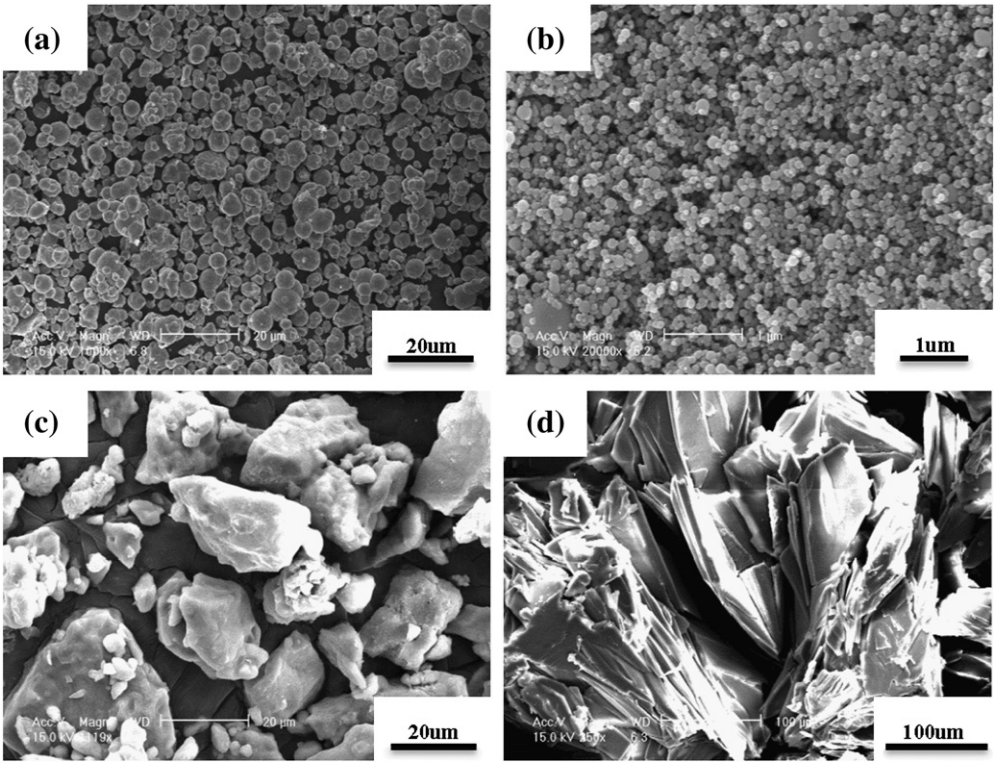

Fig. 1. FE-SEM micrographs of the raw materials: (a) iron powders, (b) nickel powders, (c) sulfur powders and (d) stearic acid.

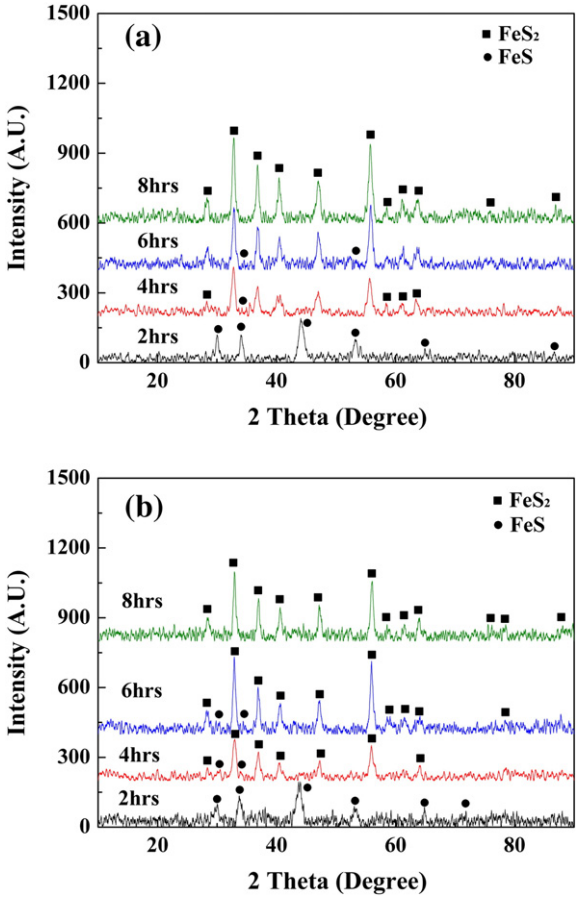

Fig. 2. XRD patterns of mechanically alloyed $Fe_{0.8}Ni_{0.2}S_2$ (a) and $Fe_{0.9}Ni_{0.1}S_2$ (b) with different milling times.

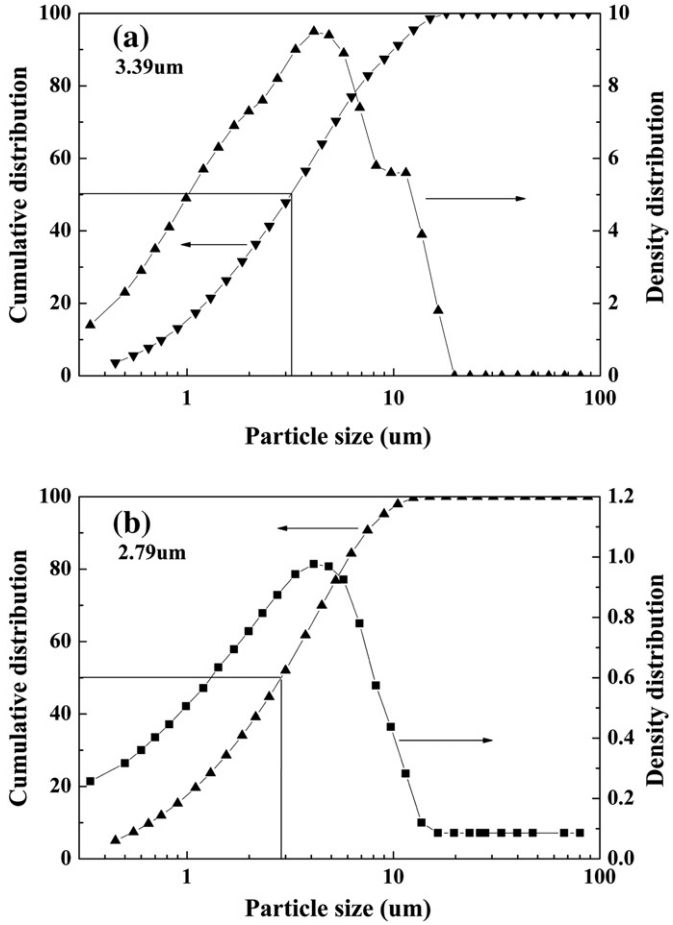

Fig. 3. Density distribution and cumulative distribution curves of synthesized $Fe_{0.8}Ni_{0.2}S_2$ (a) and $Fe_{0.9}Ni_{0.1}S_2$ (b) powder particles.

2. Experimental

2.1. Synthesis of Ni-doped FeS_2

In order to study the charge/discharge properties and cycle life of Li/Ni-doped FeS_2 cells, pure iron powders (99.9%, <10 μm), nickel powders (99.9%, nanometer) and sulfur powders (99.5%, −100 mesh) were dried in an oven at 60 °C for 24 h. According to the chemical formula for iron disulfide, the atomic percent of iron, nickel and sulfur was set at 8:2:20 and 9:1:20, respectively, to prepare two kinds of cathode materials with different nickel doping contents (these two cathode materials were named $Fe_{0.8}Ni_{0.2}S_2$ and $Fe_{0.9}Ni_{0.1}S_2$, respectively, based on their atomic ratios). In addition, the same quantity of stearic acid ($CH_3(CH_2)_{16}CO_2H$) was added during the milling process, as a kind of process control agent (PCA), as it can prevent excessive cold welding and severe agglomeration from occurring during the process of mechanical alloying. In addition, the same type of grinding media (stainless steel balls, 5 mm) was used, and the ball powder ratio (BPR) was kept constant at 20:1 during the whole milling time. Meanwhile, all mixture handling (loading and un-loading) was done in an argon-filled glove box to avoid oxidation. Actually, in this study, with the aim of avoiding instantaneously excessive heat generation (this can occur not only from the chemical reaction between iron and sulfur, but also from collisions between balls, or balls and the interior wall surface), half the amount of sulfur was added first, and after 2 h, the remaining amount was added, and the milling processes were performed for up to 8 h with an SPEX Mill (SM) at a high rotating speed of 1000 rpm.

2.2. Preparation of cathodes and anodes

To fabricate Ni-doped FeS_2 cathodes, active materials (two kinds of synthesized Ni-doped FeS_2, 60 wt.%), PEO (polyethylene oxide, 20 wt.%), Super-P (MMM carbon, 20 wt.%) and ACN (acrylonitrile) were mixed uniformly first, then the prepared slurries were pasted on an aluminum foil at room temperature using the doctor-blade casting method. In addition, with the aim of comparing the electrochemical properties of both of these Li/Ni-doped FeS_2 cells, the cathodes were both manufactured by planetary ball milling (PBM) at a speed of 300 rpm for 3 h, and the prepared films were dried at 80 °C for 24 h in an air oven, and then cut into disk electrodes (~1.1 cm in diameter) and stored in an argon-filled glove box. Meanwhile, lithium foils (Aldrich Chem. Co.) were also sliced into disks (~1.1 cm in diameter) and used as the anodes in this experiment.

2.3. Preparation of electrolyte

The same electrolyte was used for all tests by dissolving 1 M (lithium trifluoromethanesulfonate, Aldrich Chem. Co.) $LiCF_3SO_3$ salt in a liquid of TEGDME (tetraethylene glycol dimethyl ether, Aldrich Chem. Co.).

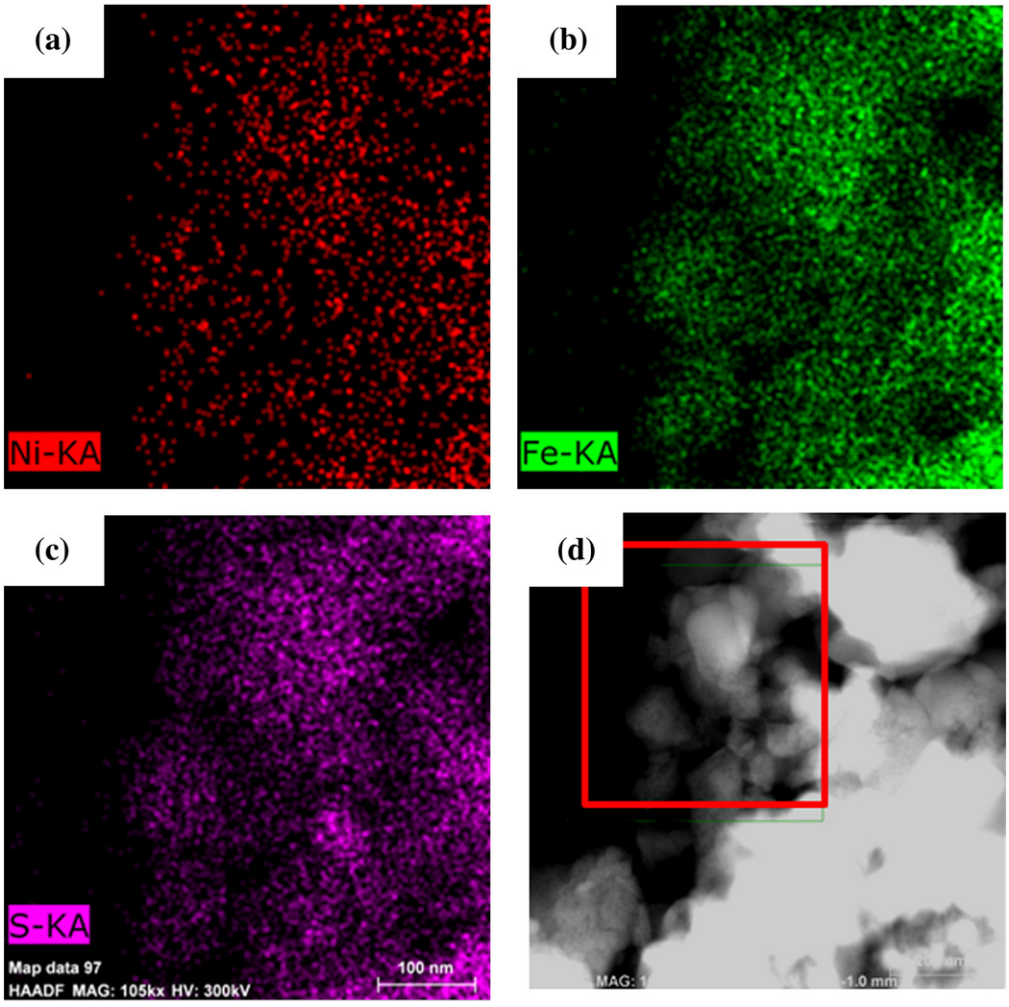

Fig. 4. TEM micrographs and EDS mapping results (in the red part of the box) of synthesized $Fe_{0.8}Ni_{0.2}S_2$ in the STEM module.

2.4. Assessment and measurement

In this study, field emission scanning electron microscopy (FE-SEM) and transmission electron microscopy (TEM) were used to investigate the surface morphologies of the powder particles and cathode surfaces, and X-ray diffraction (XRD) was conducted to examine the crystal structure and composition of the synthesized compounds. The experimental diffraction patterns were collected with a scanning step of 0.02° at a range of $10° < 2\theta < 90°$ using a graphite monochromator. In addition, an energy-dispersive X-ray spectrometer (EDS) was used to perform chemical analysis in both FE-SEM and scanning transmission electron microscopy (STEM) and map the surface image of the cathodes at different stages. HELOS Particle Size Analysis was used to measure the mean particle size of the mechanical alloyed compounds after the whole milling process. A WBCS 3000 Battery Tester (WonA Tech) was used to study the electrochemical properties of both Li/Ni-doped FeS_2 cells at normal temperature and electrochemical impedance spectroscopy (EIS) (CMS100, Gamry Instruments Inc.) was conducted to evaluate changes in the interfacial resistance occurring during the charge/discharge process.

3. Results and discussion

Fig. 1 shows the FE-SEM images of the starting elements used in this experiment. The spherical iron and nickel powders shown in Fig. 1a and b both have a good size distribution with a mean particle size of 7 μm and 160 nm, respectively. Meanwhile, micrographs of the soft sulfur and papery stearic acid particles are also shown in Fig. 1c and d, respectively.

As is known, the ball milling procedure used here is a mechanical alloying process, in which the powder particles were repeatedly flattened, cold welded, fractured and re-welded, resulting in the generation of a variety of crystal defects, such as dislocations, stacking faults, and vacancies. As the balance between cold welding and fracturing of the powder particles is responsible for changes in the crystal structure and size distribution, in this study, half of the sulfur is added to the milling vial at the beginning, to reduce the heat emitted instantly from the chemical reactions with iron (when 1 mol condensed FeS forms at 298.15 K, approximately 119.656 kJ of heat will be released, while approximately 171.544 kJ per mole of FeS_2 under the same conditions; referenced from the Thermochemical Data of Pure Substances [9]), and also to decrease the phenomena of excessive cold welding and powder agglomeration during the whole milling process.

Phase transformations of $Fe_{0.8}Ni_{0.2}S_2$ and $Fe_{0.9}Ni_{0.1}S_2$ during the whole milling process were completely recorded and displayed using the XRD patterns presented in Fig. 2a and b, respectively. As shown, the following information can be obtained: after 2 h of ball milling, FeS (JCPDS card No. 89-6926) was formed firstly by consuming most of the starting materials of iron and sulfur; however, peaks of nickel or nickel sulfides weren't detected. There are two possibilities for this: raw nickel may have replaced some iron atoms in the FeS lattice, or the nickel content was too low to determine through XRD. In addition, after the residual sulfur was added and milled for 4 h, almost identical XRD patterns can be seen in both Fig. 2(a) and (b), where most of the

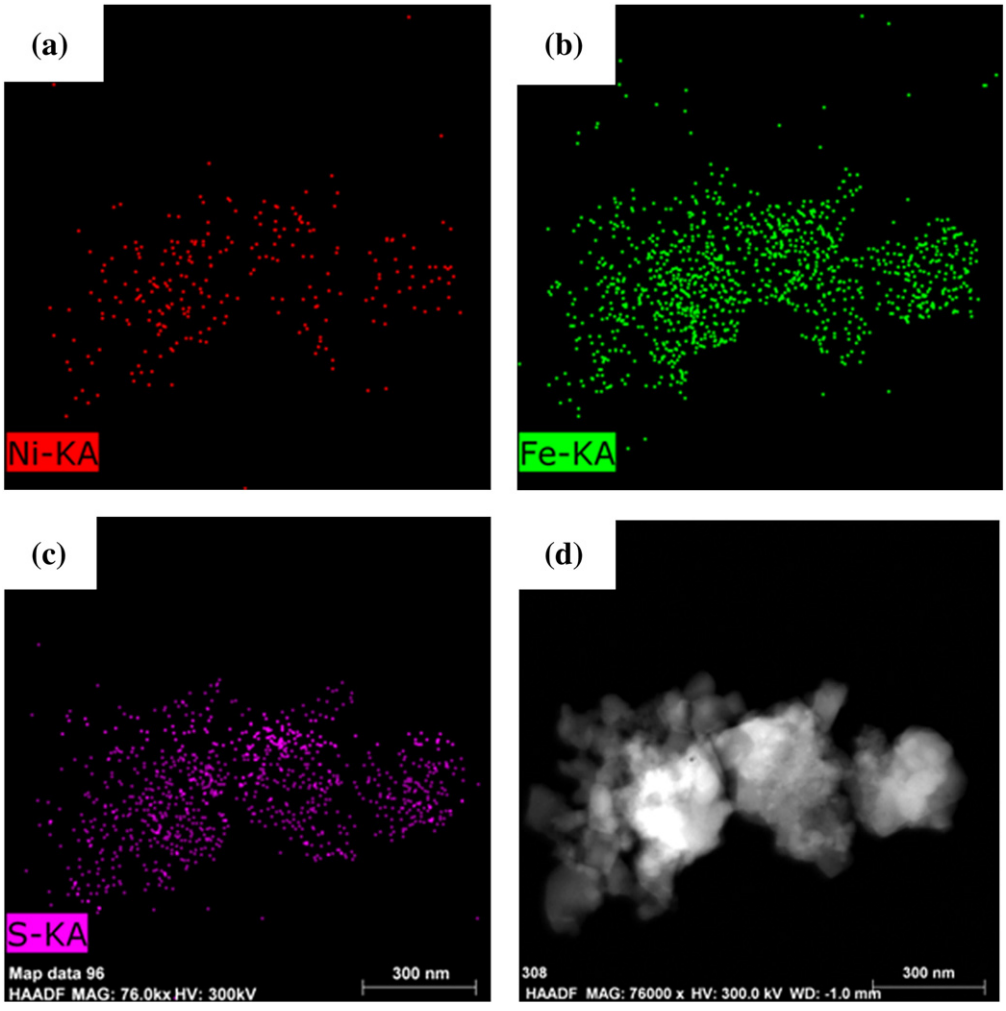

Fig. 5. TEM micrographs and EDS mapping results of synthesized $Fe_{0.9}Ni_{0.1}S_2$ in the STEM module.

FeS_2 peaks replaced the original FeS position, mainly due to the heavy plastic deformation, which can strongly induce explosive reactions between the new generated FeS and the residual sulfur. Finally, in order to obtain high-purity FeS_2 with a small mean particle size, the milling time was extended to 8 h, and patterns, in close agreement with the representative cubic iron disulfide phase (JCPDS card No. 71-2219), were obtained.

Previous research reports showed that better size distribution could provide larger contact areas between the active materials, then Li-ions' diffusion path could be shortened and the cycle life could be improved [5,6]. Therefore, analysis of the cumulative and density distribution of alloyed $Fe_{0.8}Ni_{0.2}S_2$ and $Fe_{0.9}Ni_{0.1}S_2$ powder particles was performed and is shown in Fig. 3a and b, respectively. As is known, for the same substance, the density distribution curve characterizes its size distribution, and the abscissa value of the particle size corresponding to the ordinate value of 50% of the cumulative distribution represents its mean particle size. In this study, the density distribution curves of $Fe_{0.8}Ni_{0.2}S_2$ and $Fe_{0.9}Ni_{0.1}S_2$ are very similar to each other; both have only one broad peak around their mean particle size of 3.39 μm and 2.79 μm, respectively, not only demonstrating their good size distribution, but also indicating further good electrochemical properties of Li-ion cells.

Figs. 4 and 5 show the TEM micrographs and EDS mapping results (detected in a STEM module) of synthesized $Fe_{0.8}Ni_{0.2}S_2$ and $Fe_{0.9}Ni_{0.1}S_2$ powder particles, respectively. Clearly, the elements of iron and sulfur are both well distributed on the surface of the iron disulfide powders. In order to analyze the situation of nickel doping, the atomic percent of the constituents was also tested, and the results showed that the sulfur, iron, and nickel content was 58.62%, 33.26%, and 8.12% and 59.64%, 36.29%, and 4.07%, respectively, for the $Fe_{0.8}Ni_{0.2}S_2$ and $Fe_{0.9}Ni_{0.1}S_2$ powder particles. According to the chemical formula for iron disulfide, the ratio of sulfur to iron is less than its theoretical value, approximately 1.76 and 1.64, respectively, which may be due to the lack of sulfur, since it is soft and easily adheres to the interface of the milling jar during MA. Furthermore, it can be verified that the nickel has been well doped in the iron disulfides from its good distribution on the surfaces of the alloyed $Fe_{0.8}Ni_{0.2}S_2$ and $Fe_{0.9}Ni_{0.1}S_2$ particles.

In the charge/discharge process, all test conditions were kept constant, except for the voltage range (between 0.4 and 2.8 V or between 0.8 and 2.4 V) and current density (0.1 C, 0.2 C or 0.5 C), to reduce experimental error as much as possible. Since the setting of the voltage range has an important impact on the electrochemical properties of the cells measured, in this study, the initial charge/discharge curves of the Li/$Fe_{0.8}Ni_{0.2}S_2$ cells with voltages ranging from 0.4 to 2.8 V and 0.8 to 2.4 V are shown in Figs. 6a and 7a, respectively. For the former, four redox reactions separately occurred at the I, II, III and IV regions, and the corresponding chemical reaction formulas are presented in Table 1. Meanwhile, after nickel doping, the potential of the first discharge plateau increased greatly from the original 1.1 V [10,11] to 1.6 V, indicating its lower ohmic loss during the initial reduction process. However, after the formation of sulfur at approximately 2.6 V during the first charge process, a series of high-order polysulfides (such as Li_2S_8 and Li_2S_6) were generated and dissolved in the electrolyte during the subsequent discharge, and further spread to the anode, reacting with the lithium metal directly to form low-order polysulfides such as

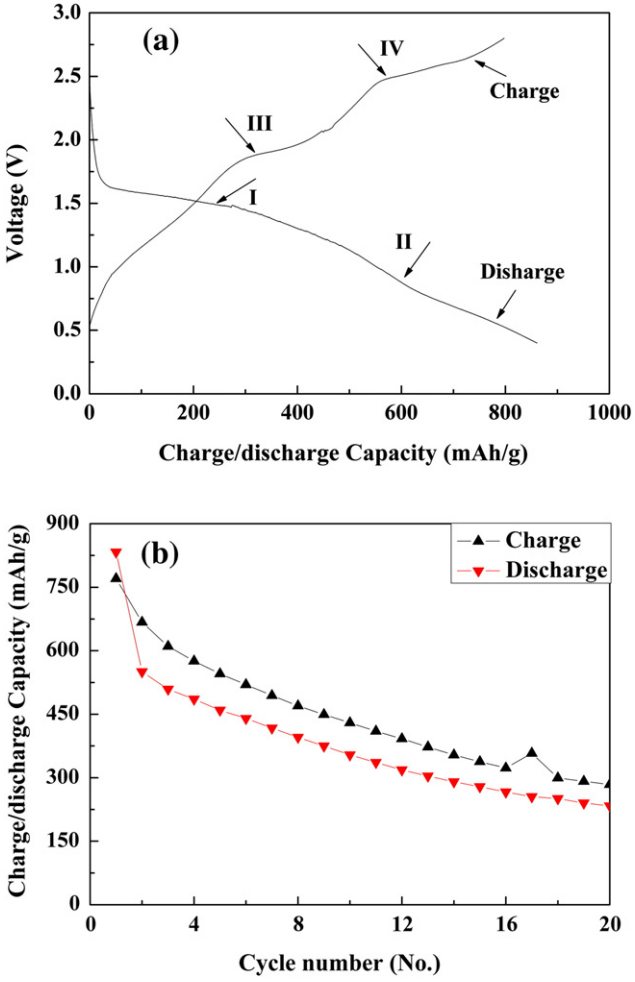

Fig. 6. Initial charge/discharge curves (a) and cycle performance (b) of Li/$Fe_{0.8}Ni_{0.2}S_2$ cells tested ranging from 0.4 to 2.8 V at 0.1 C at room temperature.

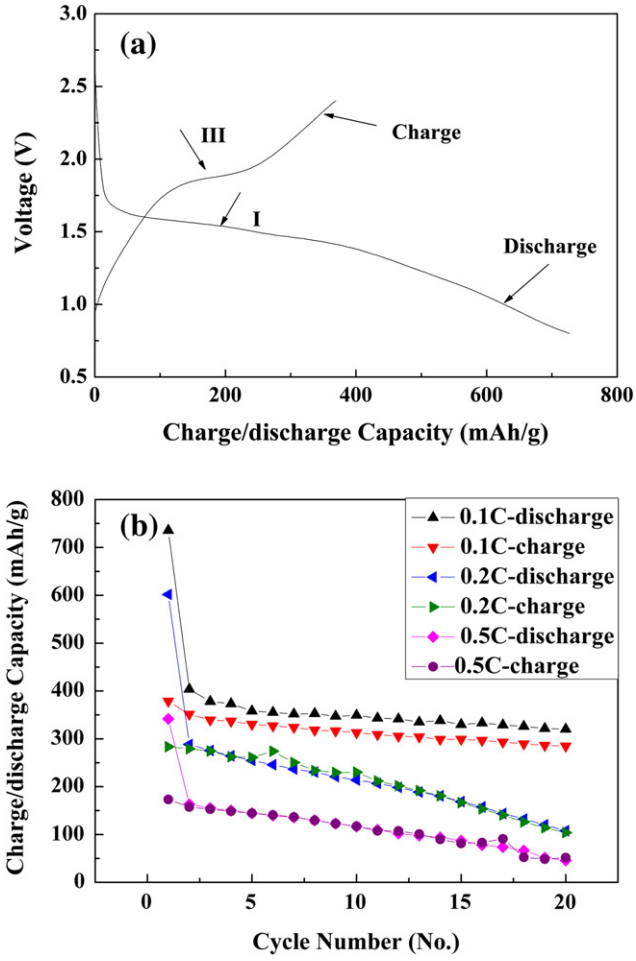

Fig. 7. Initial charge/discharge curves at 0.1 C (a) and cycle performance (b) of Li/$Fe_{0.8}Ni_{0.2}S_2$ cells tested ranging from 0.8 to 2.4 V at room temperature.

Table 1
The electrochemical reactions occurring in Li/FeS_2 cells during the first charge/discharge process.

Electrode	Cycle	Process	Reactions	Peak potential	Ref.
Ni-doped FeS_2 cathode	First cycle	Reduction	I: $FeS_2 + 4Li \rightarrow Fe + 2Li_2S$	1.1 V	[10,11]
			II: $Fe + xLi \rightarrow Li_xFe$ or $C + xLi \rightarrow Li_xC$	~0.8 V	[12]
		Oxidation	III: $2Li_2S + Fe\text{-}2Li \rightarrow FeS + Li_2S$	1.9 V	[13,12]
			IV: $Li_2S\text{-}2Li \rightarrow S$	2.6 V	[12,14]

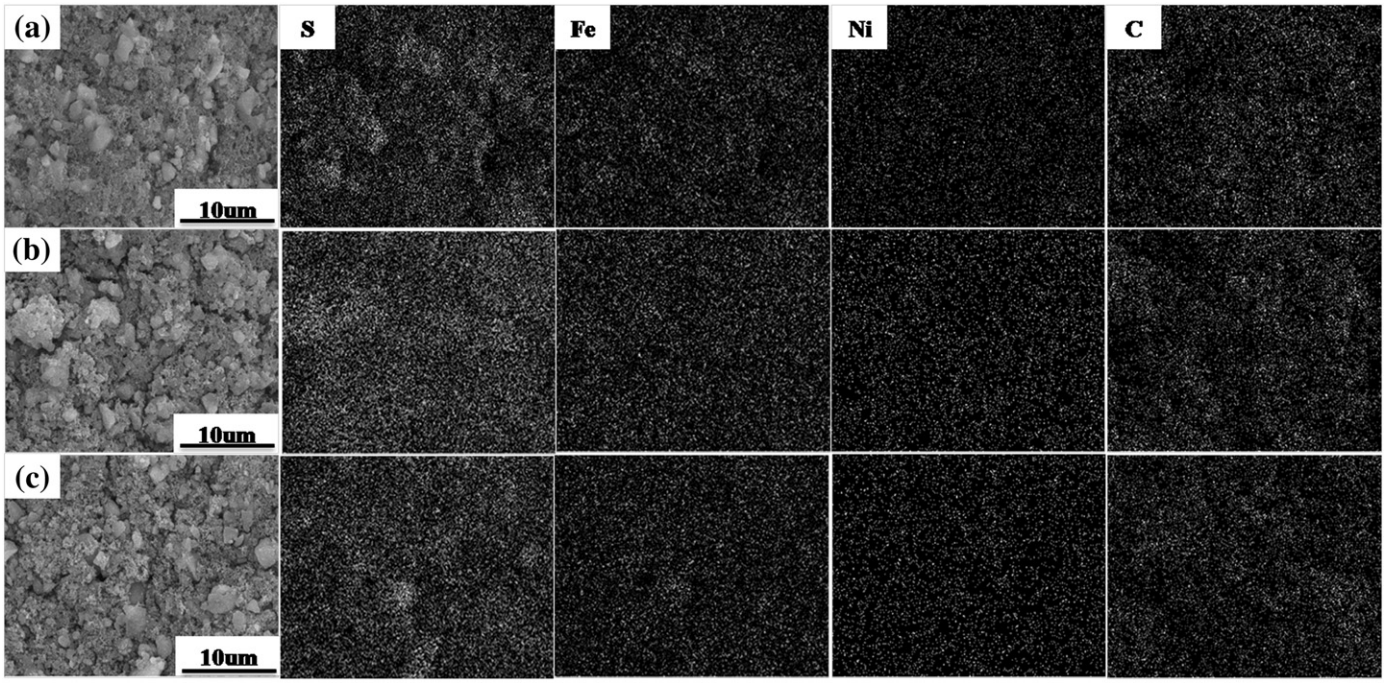

Fig. 8. FE-SEM and EDS mapping photos of cathode in Li/$Fe_{0.8}Ni_{0.2}S_2$ cell before (a) and after first discharge (b)/charge (c) process.

Li_2S_2 and Li_2S. During the corresponding charge process, polysulfides dissolved in the electrolyte can diffuse back to the cathode surface and participate in the oxidation reaction, and continue to shuttle. This phenomenon is called the charge-protection shuttle, and can be expressed by the following reaction [15]:

$$Li^+ + nS - - Li_2S_n \ (n>4).$$

Since its presence may result in active material loss, an increase in the viscosity of the liquid electrolyte, or even deterioration of the cells measured, the cutoff voltage (COV) was reset, from 0.8 V (avoiding the chemical reaction occurring at region II) to 2.4 V, and applied to all the following tests. As shown, Li/$Fe_{0.8}Ni_{0.2}S_2$ cells tested between 0.4 and 2.8 V displayed an initial charge/discharge capacity of 770/832 mAh/g, much higher than the one from 0.8 to 2.4 V (726/369 mAh/g). However, its cycle life shown in Fig. 6b is extremely bad, with a lower charge/discharge capacity of 284/233 mAh/g after 20 cycles compared with the latter (320/285 mAh/g), shown in Fig. 7b. Meanwhile, its capacity decay rate is also much faster than the latter; therefore, it is worth noting that avoiding reactions II and IV can help greatly in improving all electrochemical properties of Li/$Fe_{0.8}Ni_{0.2}S_2$ cells. In addition, cycle performances with a current density of 0.2 C and 0.5 C were also investigated for up to 20 cycles at room temperature, as shown in Fig. 7b; the higher the current density used, the higher the ohmic resistance, and the lower the capacity, the worse the cycle life.

Fig. 8 shows the FE-SEM micrographs and EDS mapping results for the $Fe_{0.8}Ni_{0.2}S_2$ cathode before (a) and after the 1st discharge (b)/charge process (c), respectively. As shown, $Fe_{0.8}Ni_{0.2}S_2$ particles, ranging from submicron to 3.5 μm, were dispersed well in the mixture before cycling. In addition the elements of iron, sulfur, nickel and carbon are all well distributed on the surface of the cathode. After the 1st discharge, the electrode surface cracked, and the phenomenon of particle agglomeration occurred. In terms of chemical reactions, most of the gathered mass might be composed of the final reduction product of Li_2S, which can be verified by analyzing both the iron and sulfur mapping graphs together. In addition, as the 1st charge process finished, the agglomerated particles disappeared, but not the existing cracks, indicating that only part of the reduction product participated in the reaction during the oxidation process, consistent with the given chemical reaction equation.

In order to detailedly analyze the element content, EDS mapping results of the $Fe_{0.8}Ni_{0.2}S_2$ cathode before and after the 1st discharge/charge are presented in Table 2. In fact, these results largely depend on the state of the cathode surface and can only provide some basis for the following quantitative analysis, because EDS is only suitable for detecting the outermost layer of the measured materials. Clearly, regardless of the form of sulfur and iron present (simple substance or compound), after all the reduction–oxidation reactions, their contents changed little, indicating no loss of active materials during the entire test. Meanwhile, the deviation existing between the actual measured

Table 2
The EDS mapping results (atomic ratio) of $Fe_{0.8}Ni_{0.2}S_2$ cathodes at different stages.

	Before test	After 1st discharge	After 1st charge	Theoretical value
S	58.99	58.45	58.56	66.7
Fe	33.17	33.11	33.15	26.7
Ni	7.84	8.44	8.29	6.6
S/(Fe + Ni)	1.44	1.41	1.38	2
Fe/Ni	4.23	3.92	4	4

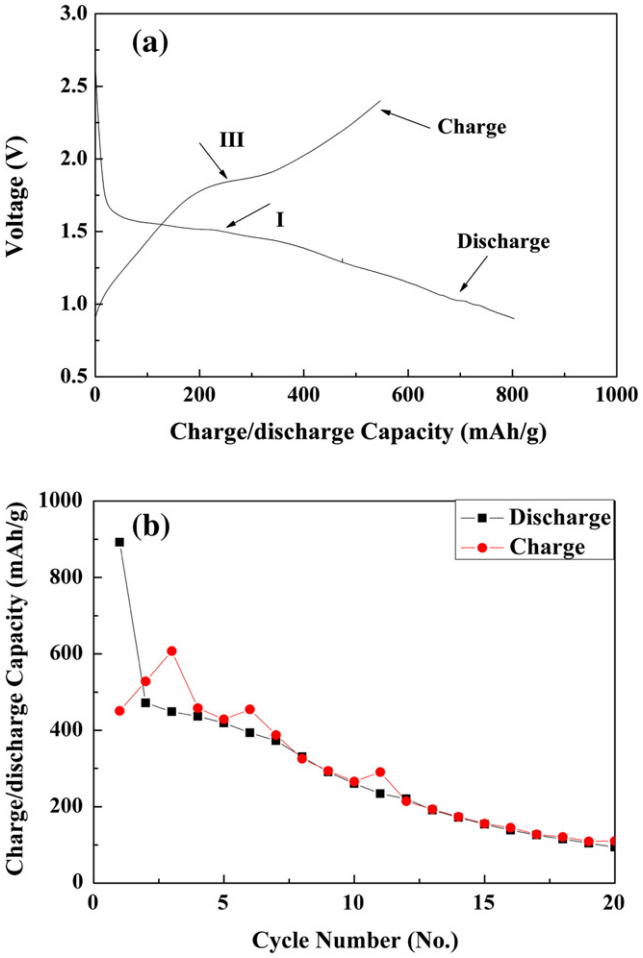

Fig. 9. Initial charge/discharge curves (a) and cycle performance (b) of Li/$Fe_{0.9}Ni_{0.1}S_2$ cells tested ranging from 0.4 to 2.8 V at 0.1 C at room temperature.

Table 3
The EDS mapping results (atomic ratio) of $Fe_{0.9}Ni_{0.1}S_2$ cathodes at different stages.

	Before test	After 1st discharge	After 1st charge	Theoretical value
S	59.24	59.6	58.86	66.7
Fe	36.37	36.19	36.74	30
Ni	4.4	4.21	4.4	3.3
S/(Fe + Ni)	1.45	1.3	1.36	2
Fe/Ni	8.26	8.59	8.35	9

value and theoretical value is mainly due to the lack of sulfur, mentioned previously. However, the variation of the atomic percent of nickel (from 7.84 to 8.44, and then 8.29) during the discharge/charge process seems difficult to explain, since the mechanical alloying process is very complex. The powder particles had to go through repeated deformation and finally resulted in the generation of a variety of crystal defects, such as dislocations, stacking faults, and vacancies. Therefore, the whereabouts of the nickel element is difficult to track using existing equipment. If we suppose that nickel was compelled to replace some iron atoms and form a solid solution (nickel is the solute, and iron is the solvent) at the very beginning, and then reacted with sulfur and created iron disulfide, the fact that the actual measured atomic ratio of iron to nickel (4.23, 3.92 and 4) is almost equal to its theoretical one seems to validate the assumptions.

Similarly, the electrochemical properties of the Li/$Fe_{0.9}Ni_{0.1}S_2$ cells were also investigated to compare with the former one, as shown in Fig. 9. The initial charge/discharge capacity of 547/803 mAh/g was higher than that for Li/$Fe_{0.8}Ni_{0.2}S_2$ cells measured at the same voltage range (from 0.8 to 2.4 V), however, its cycle life seemed relatively poor, with less than 20% of the original charge/discharge capacity after 20 cycles. This is mainly due to the formation of different redox products, which deteriorated the surface of the active materials and immensely influenced lithium diffusion and the reutilization of favorable reaction substances.

In addition, the FE-SEM micrographs and EDS mapping results for the $Fe_{0.9}Ni_{0.1}S_2$ cathode before (a) and after the 1st discharge (b)/charge process (c) are also presented in Fig. 10, respectively. As was the case

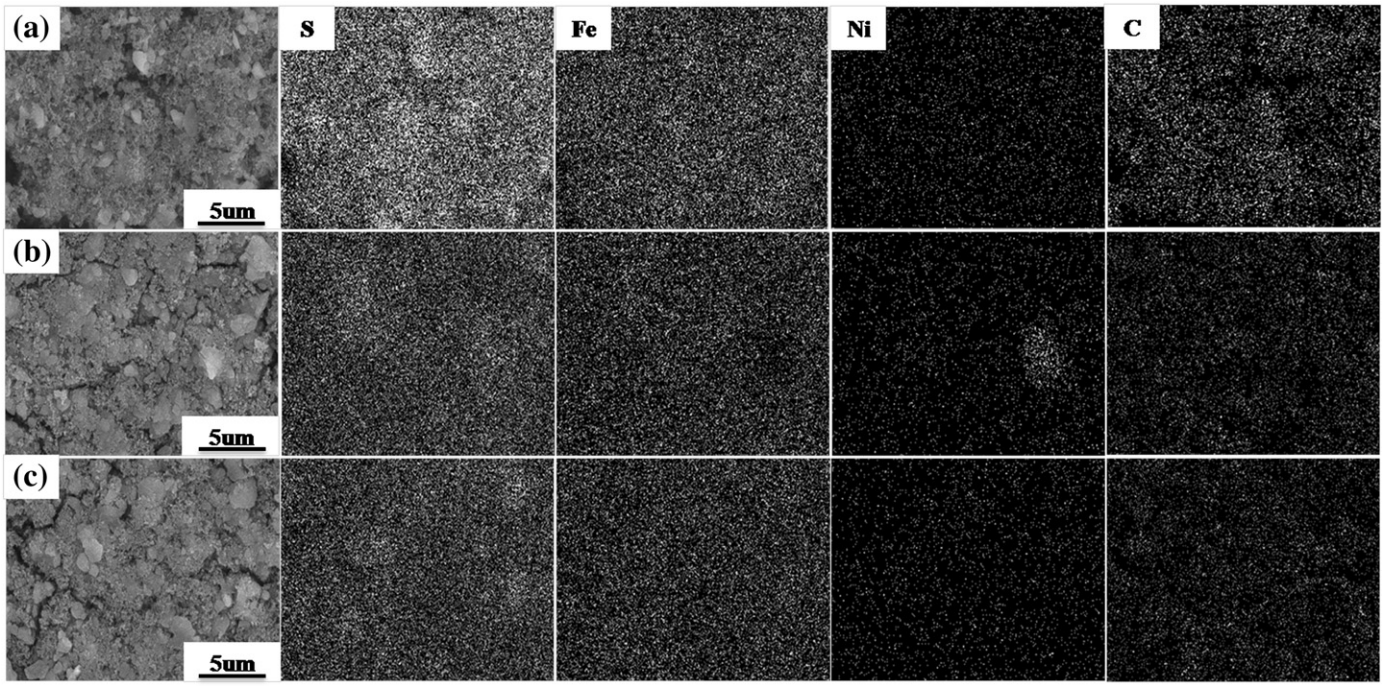

Fig. 10. FE-SEM and EDS mapping photos of cathode in Li/$Fe_{0.9}Ni_{0.1}S_2$ cell before (a) and after first discharge (b)/charge (c) process.

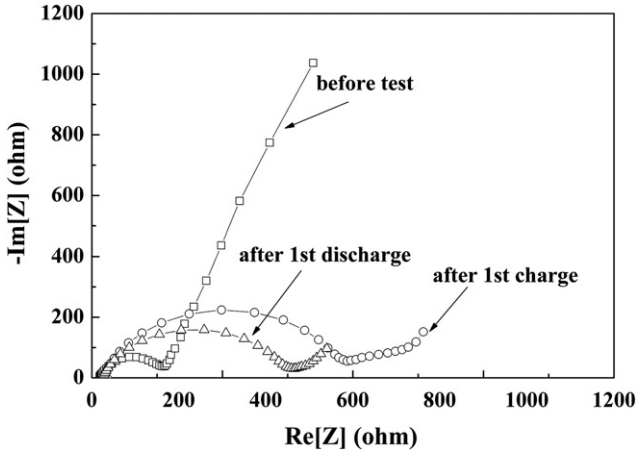

Fig. 11. AC impedance spectra of $Fe_{0.8}Ni_{0.2}S_2$ cathode before and after first charge/discharge process.

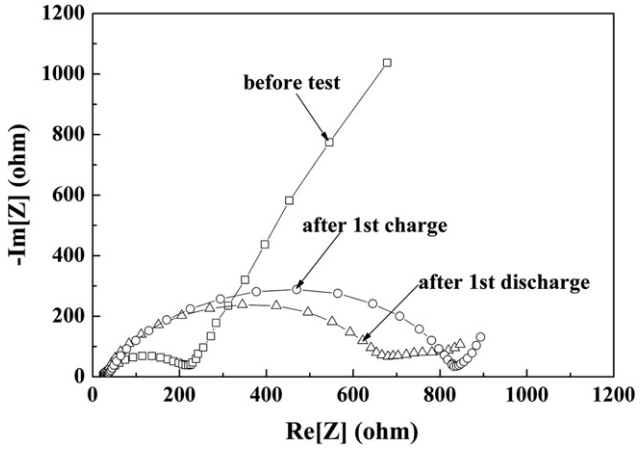

Fig. 12. AC impedance spectra of $Fe_{0.9}Ni_{0.1}S_2$ cathode before and after first charge/discharge process.

with the $Fe_{0.8}Ni_{0.2}S_2$ cathode, before cycling, the conductor, binder and active materials were uniformly mixed together with each other, and the outer layer has a large amount of micropores, which can help with the fast penetration of the electrolyte, to further accelerate the diffusion rate of Li-ions to the interior of the active materials. After the 1st discharge, the micropores almost disappeared and the cathode surface seemed condensed but with some cracks. Even more importantly, the reduction of nickel sulfide was determined by virtue of the mapping graphs (S, Fe and Ni shown in (b)). There may be many reasons for this; if the nickel doping position is unstable or the local doping content is too high, during the reduction reaction, nickel sulfide may be generated and measured by EDS, or perhaps, at the very beginning of the mechanical alloying, the nickel didn't form a solid solution with iron, but reacted directly with sulfur. After the discharge process, it is likely to be restored to nickel sulfide. Finally, from the mapping graph of (c), sulfur, iron and nickel are all well distributed on the surface of the cathode, without nickel sulfide compounds. However, the cracks still existed and seemed more serious, due to the frequent intercalation and deintercalation of lithium ions between the active materials. The EDS mapping results for the $Fe_{0.9}Ni_{0.1}S_2$ cathode before and after the 1st discharge/charge are also presented in Table 3. As shown, the fact that there was no loss of active materials after the discharge/charge test can be demonstrated by examining the mapping results, which show that the atomic fractions of sulfur and iron changed little from the original ones.

To understand the reason for the electrochemical performance of the nickel-doped FeS_2 composites synthesized using a mechanical alloying process, EIS was also carried out (in the frequency range of 100 mHz–1 MHz, at an alternating current (AC) voltage of 10 mV) to measure the lithium-ion diffusion resistance in the $Li/Fe_{0.9}Ni_{0.1}S_2$ and $Li/Fe_{0.8}Ni_{0.2}S_2$ cells at room temperature, respectively, presented by the Nyquist profiles shown in both Figs. 11 and 12. The electrolyte resistance was estimated from the intersection of the front end of the semicircles with the abscissa axis, which is similar for both cathodes due to the same electrolyte being used. The diameter of the impedance semicircles is related to the charge transfer resistance, approximately controlled by the stage of the electrochemical reactions occurring on the cathode surfaces. Clearly, before cycling, both cathodes have a slightly lower charge transfer resistance value; however, after the first charge/discharge process, the transfer resistance seemed to have obviously increased for both, especially the $Li/Fe_{0.9}Ni_{0.1}S_2$ cell. This is expected due to its lower first charge/discharge capacity compared to the $Li/Fe_{0.8}Ni_{0.2}S_2$ cell, mainly due to its good doping, and hence improving its electronic conductivity.

4. Conclusions

Iron disulfide-based cathode materials with different nickel doping contents were synthesized by mechanical alloying using a high-energy milling machine. In addition to the size distribution, crystallinity and purity, the test conditions can also significantly affect the cycling properties. Meanwhile, it was suggested that the improvement of the cycling stability and the enhanced electronic conductivity were mainly attributed to the higher nickel doping content, presenting us with a new, simple and low-cost method to prepare various beneficial electrode materials.

Acknowledgments

This research was supported by the Basic Science Research Program (2009-0071729) and the WCU Program (R32-20093) through the National Research Foundation of Korea (NRF) and Ministry of Education, Science and Technology.

References

[1] Y.P. Wu, H.P. Zhang, F. Wu, C.H. Li, Polymer lithium ion batteries, Chemical Industry Press, Beijing, 2006. 104–110.
[2] D. Cherns, G.P. Ngo, J. Solid State Chem. 50 (1983) 7.
[3] Y. Han, Y.P. Wang, W.H. Gao, Y.J. Wang, L.F. Jiao, H.T. Yuan, S.X. Liu, Powder Technol. 212 (2011) 64.
[4] X.J. Liu, S.D. Kang, J.S. Kim, H.J. Ahn, S.G. Lim, I.S. Ahn, Rare Metals 30 (2011) 5.
[5] X.J. Liu, S.D. Kang, J.S. Kim, I.S. Ahn, H.J. Ahn, J. Nanosci. Nanotechnol. 12 (2012) 1.
[6] J.W. Choi, G. Cheruvally, H.J. Ahn, K.W. Kim, J.H. Ahn, J. Power Sources 163 (2006) 158.
[7] T.B. Kim, W.H. Jung, H.S. Ryu, K.M. Kim, J.H. Ahn, J. Alloys Compd. 449 (2008) 304.
[8] F. Disma, L. Aymard, L. Dupont, J.M. Tarascon, J. Electrochem. Soc. 143 (1996) 3959.
[9] I. Barin, S. Fried, S.R. Ernst, W.S. Sheng, Thermochemical data of pure substances, Weinheim (2009) 576–578.
[10] E. Strauss, D. Golodnitsky, E. Peled, J. Solid State Electrochem. 6 (2002) 468.
[11] K. Hansen, K. West, Electrochem. Soc. Proc. 97 (1997) 124.
[12] L.A. Montoro, J.M. Rosolen, J.H. Shin, S. Passerini, Electrochim. Acta 49 (2004) 3419.
[13] L.A. Montoro, J.M. Rosolen, Solid State Ionics 159 (2003) 233.
[14] Y.J. Choi, Y.D. Chung, C.Y. Baek, K.W. Kim, H.J. Ahn, J.H. Ahn, J. Power Sources 184 (2008) 548.
[15] X. Ji, L. Nazar, J. Mater. Chem. 20 (2010) 9821.